Sensors and Materials, Vol. 35, No. 9 (2023) 3227–3239
MYU Tokyo

S & M 3387

Miniaturized Neural Observation System for *in vivo* Brain Imaging in Freely Moving Rats

Ronnakorn Siwadamrongpong,[1†] Yoshinori Sunaga,[1†] Kiyotaka Sasagawa,[1*]
Yasumi Ohta,[1] Hironari Takehara,[1] Makito Haruta,[1,2]
Hiroyuki Tashiro,[1,3] and Jun Ohta[1]

[1]Division of Materials Science, Graduate School of Science and Technology,
Nara Institute of Science and Technology,
8916-5 Takayama, Ikoma, Nara 630-0192, Japan
[2]Department of Opto-Electronic System Engineering, Faculty of Science and Engineering,
Chitose Institute of Science and Technology,
758-65 Bibi, Chitose, Hokkaido 066-8655, Japan
[3]Department of Health Sciences, Faculty of Medical Sciences, Kyushu University,
3-1-1 Maidashi, Higashi-ku, Fukuoka 812-8582, Japan

(Received June 28, 2023; accepted September 11, 2023)

Keywords: CMOS image sensor, implantable device, brain surface imaging, *in vivo* imaging

In this study, we developed a miniaturized observation system for rat brain imaging using an implantable imager. A small data-acquisition device was designed to be mounted on the back of an adult rat, reducing the disturbance to the output of the imager caused by a long cable. With a weight of approximately 6.8 g, the movement of adult rats with an average weight of 200 g was unrestricted. The readout characteristics were evaluated at the light level. The *in vivo* experiments were performed using mice and freely moving rats. Using the developed data analysis pipeline, blood flow in the vessels was observed.

1. Introduction

The brain is a complex and important organ that requires further investigation. Brain studies at the behavioral level have explored the relationship between actions and neuronal activities in animal models resembling human cases. This information enhances the understanding and treatment of neurological disorders. Among the observation techniques, intrinsic optical imaging is employed to observe neural activities without genetic manipulation.[1,2]

Microscopy is a powerful tool for optical functional brain imaging that facilitates the observation of blood vessels and cells.[3,4] However, microscopes are generally very large and difficult to use under free-moving conditions. Technologies such as miniature microscopes, fiber bundles, and multimode fiber endoscopy have been developed for *in vivo* imaging under freely moving conditions.[5–9] Previously, as an alternative approach, we developed an ultracompact imager using our original small image sensor.[10–27] This technique reduces the invasiveness and limitation of behavior. With these advantages, we

*Corresponding author: e-mail: sasagawa@ms.naist.jp
†These authors contributed equally.
https://doi.org/10.18494/SAM4563

ISSN 0914-4935
https://myukk.org/

demonstrated deep brain imaging and simultaneously observed multiple regions of the mouse brain.[17,22] Furthermore, fluorescence imaging can be performed using an emission filter.[16,21] Multimodal measurement can be realized by combining an image sensor with another measurement device or equipment, such as a neural amplifier or microdialysis system.[25,27]

To avoid heat generation and other issues, the brain-implantable imaging device has minimal circuitry on the image sensor chip. Hence, the device output is an analog signal transmitted to an analog conversion system through a long cable. This configuration renders the system susceptible to external noise. In this study, we developed a prototype miniaturized system wherein a data acquisition device could be mounted on the back of a rat to reduce the disturbance caused by cables.

2. Miniaturized Data Acquisition System for *in vivo* Imaging

For measuring brain activity, we fabricated an image sensor system that can be mounted on the back of a rodent. This sensor is an implantable image sensor used for *in vivo* imaging and can be applied for fluorescence observations in the deep brain and blood flow measurements on the brain surface. A concept image of the system is shown in Fig. 1. In this study, we aim to achieve excellent brain surface imaging performance with a high signal-to-noise ratio (SNR).

2.1 Implantable device with CMOS image sensor

The implantable device used for brain surface imaging is the same as that previously reported. A small CMOS image sensor and six green μ-LEDs (ES-CEGHM12A, Epistar, Taiwan) are mounted on a flexible polyimide printed circuit (FPC) board and arranged in series. Figure 2(a) shows the device with μ-LEDs. The sensor is a custom-designed 120 × 268 pixel CMOS image sensor fabricated with a 0.35 μm standard CMOS process. The image sensor and its specifications are presented in Fig. 2(b) and Table 1, respectively. The pixel size is

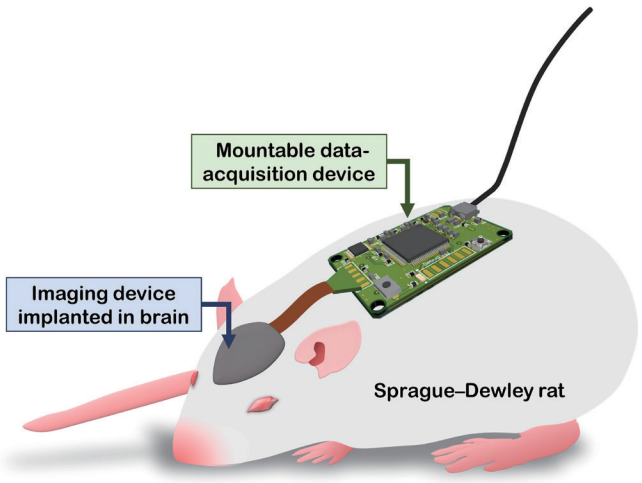

Fig. 1. (Color online) Concept of miniaturized neural observation system.

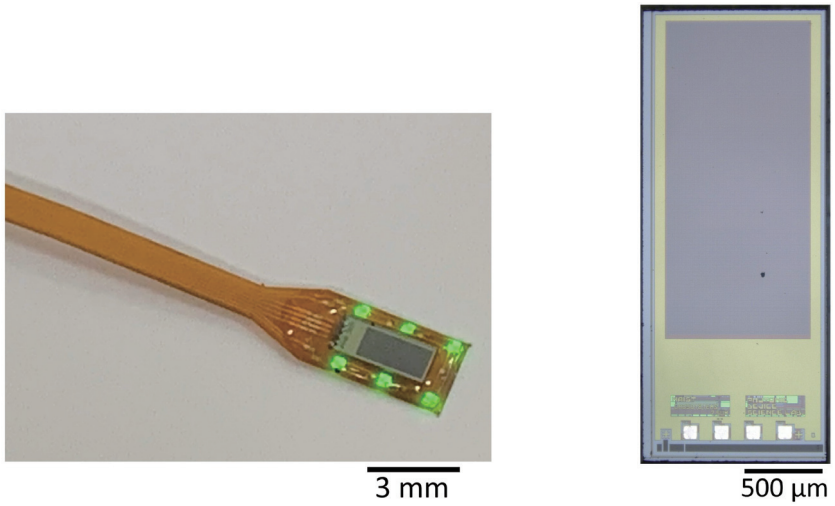

Fig. 2. (Color online) Photograph of (a) implantable device and (b) custom-designed image sensor.

Table 1
Specifications of the image sensor.

CMOS technology	0.35 µm 2-poly 4-metal standard CMOS
Operating voltage (V)	3.3
Chip size (mm^2)	1.05 × 2.90
Pixel type	three-transistor active pixel sensor
Pixel size (μm^2)	7.5 × 7.5
Pixel number	120 × 268
Photodiode	N-well/P-substrate
Fill factor (%)	44

7.5 × 7.5 μm^2, which corresponds to the imaging area of 900 × 2010 μm^2. The wavelength of µ-LEDs is 535 nm, which is highly absorbable by hemoglobin in red blood cells. The assembled device is coated with parylene-C to ensure waterproofing and biocompatibility. The lightweight cable connects the FPC to the data acquisition device and an external current source for µ-LEDs.

2.2 Data acquisition device for image sensor

The data acquisition device is designed to operate a custom-designed image sensor and to communicate with a computer through a USB. The device is shown in Fig. 3(a). It is designed as a microcontroller-based device with a size of 3.0 × 4.5 cm^2 and a weight of approximately 6.8 g. A block diagram of the device is presented in Fig. 3(b). Because a typical Sprague-Dawley rat weighs approximately 200 g, wearing this device is not expected to significantly interfere with its behavior. An ARM Cortex-M7-based microcontroller (µcontroller) (ATSAMS70N20, Microchip, USA) is used, providing a USB high-speed, a timer counter, and flexible digital and analog functions suitable for an expandable system. An external 12-bit pipeline analog-to-digital

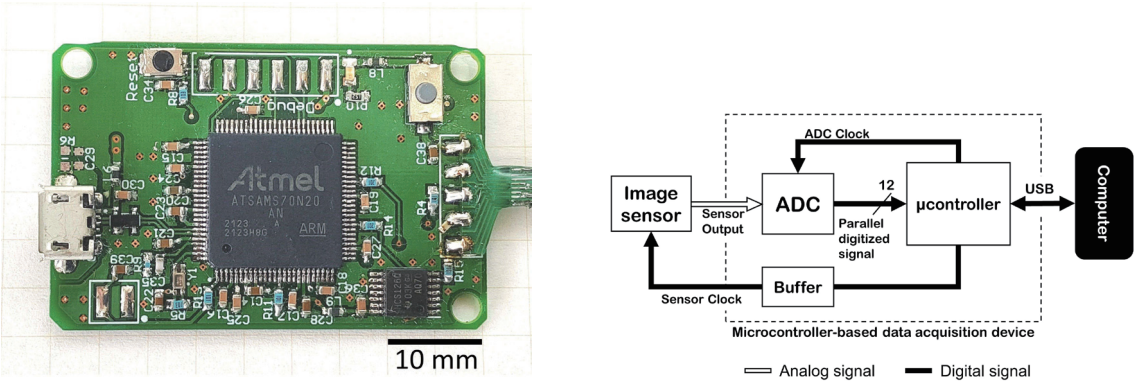

(a) (b)

Fig. 3. (Color online) (a) Image of the data acquisition device and (b) block diagram of the imaging system.

converter (ADC) (AD9235-40, Analog Device, USA) is used to achieve an average conversion speed greater than 2 Msps, which is required for brain surface imaging at 60 fps using the target image sensor.

The microcontroller firmware is designed to support image sensor operations and data management for communication. A specific header is assigned to the converted signal from ADC in unused bits and stored in the memory until data transfer. The amount of stored data is summarized and compared with the data transfer size after reading each row of pixels. This operation allows a smaller microcontroller memory to support dynamic data size and overall speed improvement with increasing variation in pixel exposure time. Finally, the pixel is read, and the device remains in the standby mode until the next frame. The interval between each row or frame is controlled by the interrupt routine service. With the designed function, the device achieves a peak conversion speed of 6.4 Msps and an average speed, including data transfer, of 3.4 Msps, corresponding to approximately 100 frames/s for the 120 × 268 pixel sensor.

2.3 Readout performance

For each light intensity, the readout performance of the data acquisition device with the custom-designed image sensor is tested at a frame rate of 60 fps. To control the light intensity in the experimental setup, a 530 nm light source (M530L4, Thorlabs, USA) and a current-controlled LED driver (DC2200, Thorlabs, USA) are used. The light intensity at each controlled current is measured using a power meter (S130VC; Thorlabs, USA). Furthermore, the output signal and temporal noise of the system are measured. Figure 4(a) shows the output signal as a function of incident light intensity. The characteristics of the output signal size are approximately linear up to a power of 6×10^{-6} W/cm^2, at which the pixels of the image sensor saturate.

The temporal noise of an imaging system can be classified into light-independent and light-dependent components. The former is caused by the pixel reset and readout circuits, whereas the latter is caused by photon shot noise. The total temporal noise σ_{tot} is given by

$$\sigma_{tot}^2 = \sigma_0^2 + \sigma_{PS}^2, \tag{1}$$

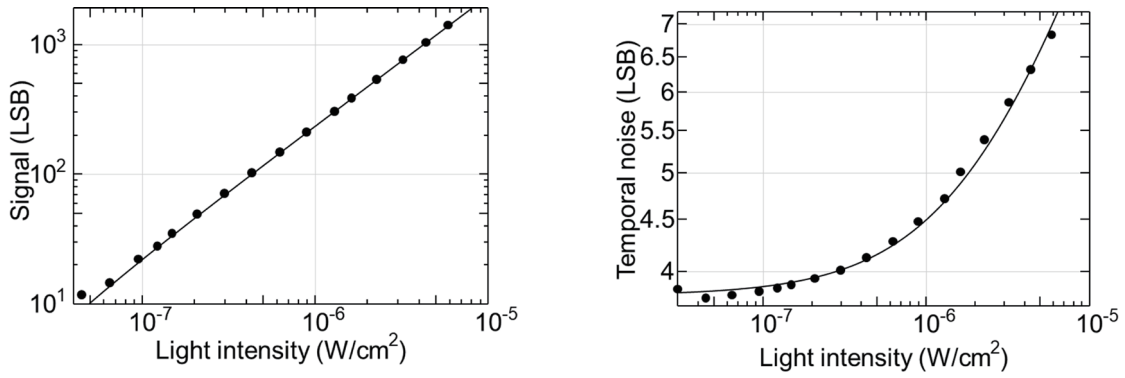

(a) (b)

Fig. 4. (a) Output signal and (b) temporal readout noise with light intensity at 60 fps. The wavelength of irradiated light is 535 nm.

where σ_0 is light-independent noise and σ_{PS} is photon shot noise proportional to the square root of the received light intensity I.

$$\sigma_{PS} \propto \sqrt{I} \tag{2}$$

Thus, the total noise is written as a function of I,

$$\sigma_{tot}^2 = \sigma_0^2 + k_{PS} I, \tag{3}$$

where k_{PS} is the coefficient of light intensity dependence.

Figure 4(b) shows a plot of the temporal readout noise with light intensity at 60 fps and a fitting line based on Eq. (3). From the fitting trend, the light-independent noise component is calculated as 3.8 LSB. At a pixel saturation of 6×10^{-6} W/cm^2, the total temporal noise is estimated to be 6.2 LSB. Compared with our previous system, these values were limited by the performance of the proposed system and can be reduced by signal processing, as discussed in Sects. 3.1 and 3.2. This system is applicable for biological imaging experiments with sufficient light levels during observation.

SNR is calculated using the measurement results, as shown in Fig. 5. According to the theory, the slope of the curve should be 20 and 10 dB/decade in the light-independent and high-light-intensity regions, respectively, and the photon shot noise is dominant in the latter.[28] For the proposed system, the photon-shot noise is dominant at sufficiently high light intensities. Consequently, the peak SNR and full-well capacity of the sensor used herein are estimated to be approximately 45 dB and 90 ke$^-$, respectively.

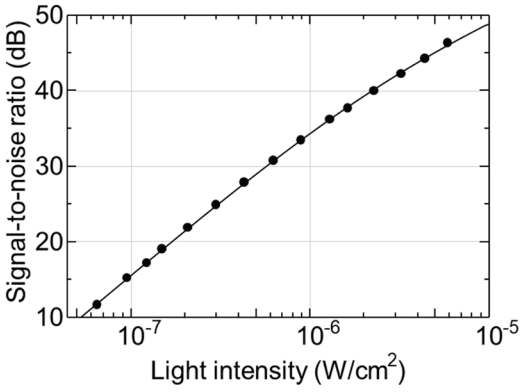

Fig. 5. SNR as a function of light intensity at 60 fps. The wavelength of irradiated light is 535 nm.

3. *in vivo* Imaging Demonstration

The prototype system is mounted on the brain surfaces of mice and rats for *in vivo* imaging experiments. All animal experiments were performed in accordance with the protocols approved by the Nara Institute of Science and Technology (NAIST).

3.1 Brain surface imaging in mouse

Compared with conventional systems, the experiments are initially conducted on adult mice (FVB/NJcl; CLEA Japan, Inc., Japan). Owing to the mouse brain surface activity, the implanted device used herein can measure blood flow velocity in blood vessels and the variation in blood volume. In this experiment, the mice were held in a stereotaxic device to confirm imaging performance. The skull is opened under urethane anesthesia and craniotomy is performed. The imaging device was inserted without removing the dura mater. During the observation period, LEDs were illuminated with a current of 0.9 mA and the frame rate was set to 92 fps. According to the previous study, a blue μ-LED powered with a current of 0.5 mA increased the surrounding brain temperature by around 0.5 °C over 1 h.[22] Operating the implantable device with the above configuration is not expected to cause any significant effect on the observed brain region.

Figure 6(a) and 6(b) show the brain surface and image captured by the sensor. The brain surface area imaged by the sensor is marked with a red rectangle. Furthermore, blood vessels on the brain surface are clearly observed in the captured images. In brain surface measurements, although the overall luminance remains constant, the blood flow information is included in the luminance variation along the blood vessel area. Therefore, the luminance difference from the reference image was obtained through image processing. Herein, the reference image is a frame-averaged image obtained throughout the measurement period. Figure 6(c) shows an example of a different image. Light and dark areas appear along the blood vessels owing to the variation in absorbance caused by the movement of red blood cells in the blood vessels.

Compared with conventional systems, the data collected from brain surface imaging have a higher noise level. Therefore, noise reduction is achieved through image processing. In Fig. 6(c),

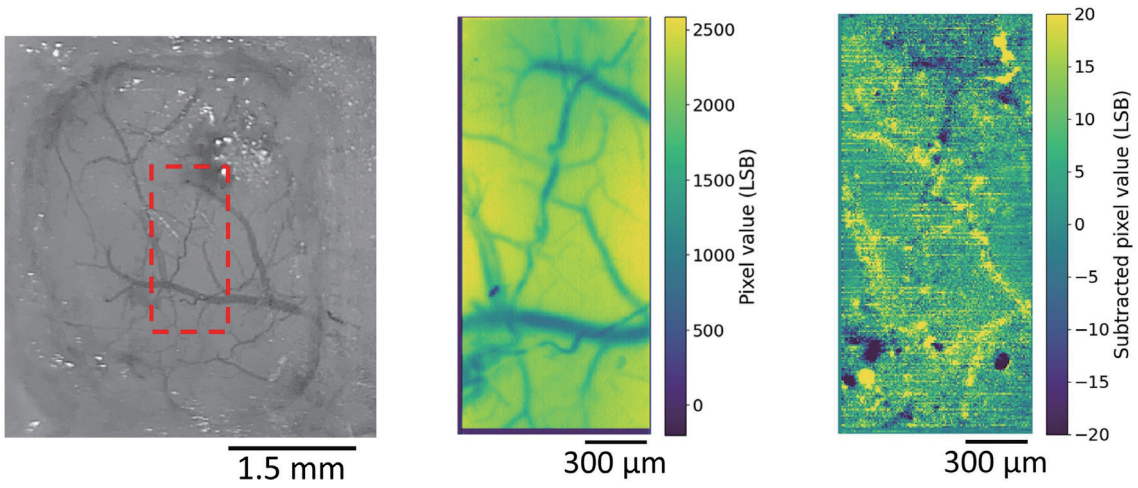

(a) (b) (c)

Fig. 6. (Color online) (a) Photograph of the mouse brain surface with imaging area indicated by the red rectangle, (b) image captured using the image sensor, and (c) difference image from the reference image.

stripe-like noise can be observed in the horizontal direction. This horizontal offset is a result of the blank time between lines varying slightly at each row owing to the microcontroller operation. While measuring the brain function, because the luminance from each frame remained fairly constant, the average pixel value for each row was calculated from 10 nearby frames and used to correct the pixel value of each row in the target frame. The resulting image is presented in Fig. 7(a).

Time-domain fluctuations from the sensor and slight movements during the observation appear in the movie data. The spectrum of each pixel is obtained using a fast Fourier transform (FFT), and the unwanted frequency components are removed.[14,23] From the collected data, high-frequency components at frequencies above 17.98 Hz are removed. Additionally, the low-frequency components between 2.89 and 2.95 Hz are removed to reduce the heartbeat noise. The images obtained after applying an inverse FFT are shown in Fig. 7(b). Furthermore, the blood flow becomes discernible after image processing. The consecutive processed images are shown in Fig. 8.

3.2 Experiments with rats under freely moving conditions

The results obtained in the aforementioned experiments with mice are in agreement with those obtained using conventional imaging devices; however, the data acquisition device in this system is not sufficiently small to facilitate the observation of free-running behavior in mice. Figure 9(a) shows the device mounted on a rat subjected to craniotomy; the imaging device is placed on the rat's head and fixed with dental cement without removing the dura mater. The brain surface is shown in Fig. 9(b).

Figure 9(c) shows an image obtained using the CMOS imaging system. A bright-field image with features similar to those in the red rectangle in Fig. 9(b) is observed. No significant noise

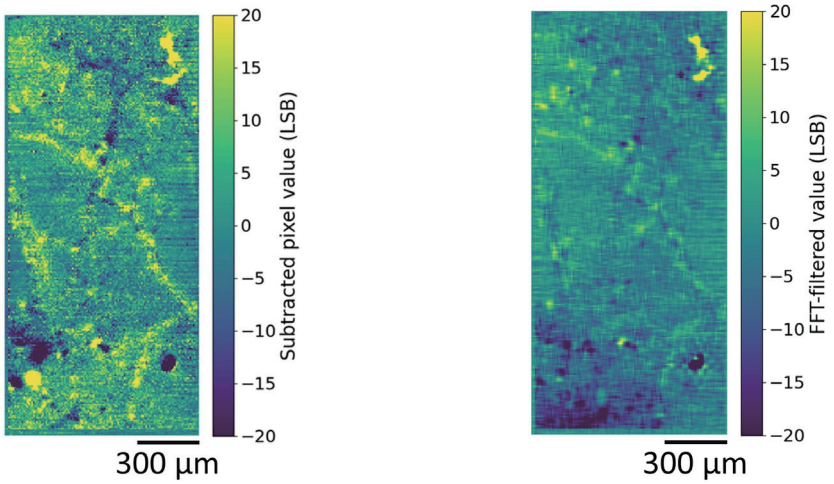

(a) (b)

Fig. 7. (Color online) Images of each processing step: (a) horizontal-line-corrected image and (b) FFT-filtered image.

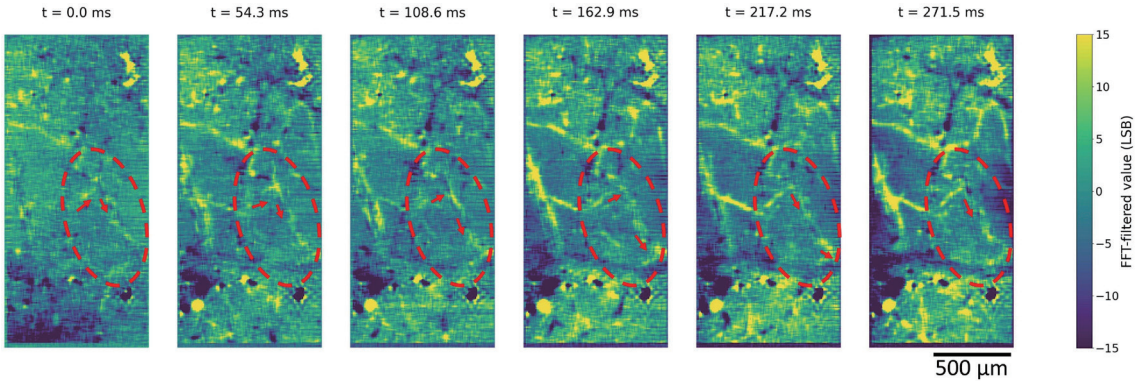

Fig. 8. (Color online) Consecutive images from data processing. The red arrow indicates the direction of blood flow.

due to disturbances caused by the rat's movement is observed. The same image processing procedure is performed on the obtained data. The horizontal and temporal noise reductions are similar to those described previously. The signal is weaker in rats because of the thicker dura mater. Therefore, a two-dimensional Fourier transform is applied to each frame to reduce the spatial high-frequency components.

The results of image processing are shown in Fig. 10. Although the signal is weak, blood flow is barely observed by image processing. The thickness of the dura mater differed between mice and rats. In our previous study, we obtained clearer images by removing the dura mater and performing measurements;[13] however, this complicates achieving stable measurements without injuring the brain surface. Alternatively, it may be possible to use a transparent artificial dura mater or apply techniques that increase the permeability of the dura mater.[29] Although the experimental duration is not demonstrated in this work, our past studies showed that observation

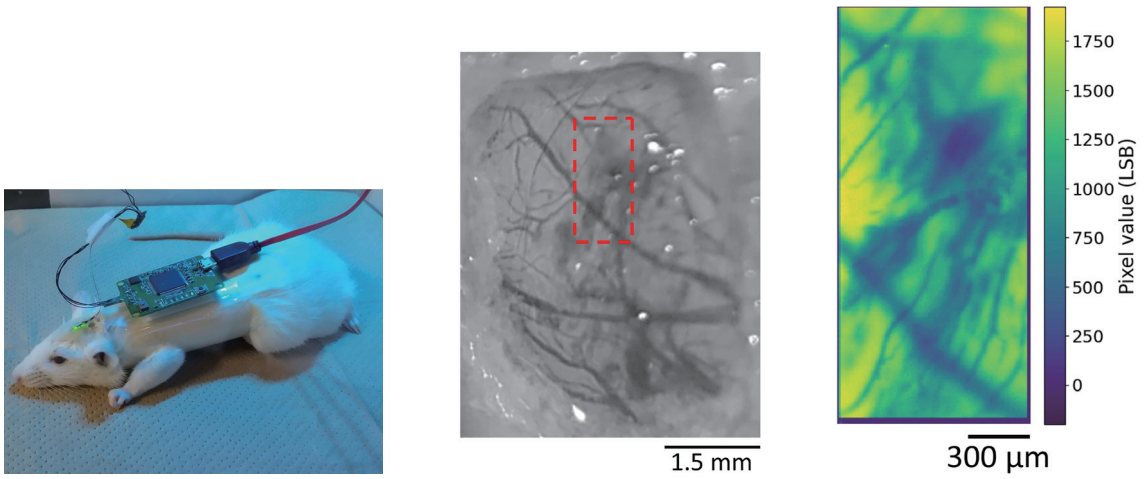

(a) (b) (c)

Fig. 9. (Color online) Photographs of (a) rat with data-acquisition device for the freely moving condition and (b) rat brain surface. The imaging area of the CMOS device is indicated by the red rectangle. (c) Image captured using the image sensor.

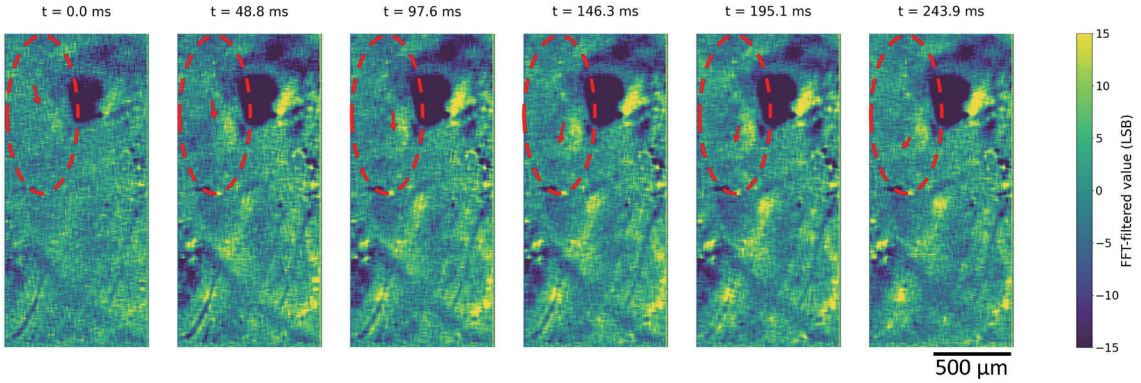

Fig. 10. (Color online) Consecutive images from data processing. The arrow indicates the direction of blood flow.

can be performed even 10 h after device implantation; this can be extended to more than one month by using a fiber-optic plate window.[13,20,24] It is expected that this system can achieve this operational duration.

4. Conclusions

In this study, we developed a neural observation system using an implantable imaging device and a small microcontroller-based data acquisition device weighing approximately 6.8 g, which is mountable on the back of an adult rat. During system evaluation, its readout characteristics were investigated with light intensity at 60 fps. The noise level was slightly greater than that of the conventional system owing to the large horizontal noise affecting it. Hence, under

the conditions of functional brain imaging, the effect of the noise was reduced by image processing. Furthermore, analog conversion was performed closer to the sensor. Additionally, mounting the circuitry for signal processing on the observable object may pave the way to further advancements in wireless communications in the future.

Acknowledgments

This work was supported by JSPS KAKENHI (Grant Numbers JP21H03809 and JP23H05450) and the VLSI Design and Education Center (VDEC), University of Tokyo, in collaboration with the Cadence Corporation and Mentor Graphics Corporation.

References

1 A. Grinvald and R. Hildesheim: Nat. Rev. Neurosci. **5** (2004) 874. https://doi.org/10.1038/nrn1536
2 E. M. C. Hillman: J. Biomed. Opt. **12** (2007) 051402. https://doi.org/10.1117/1.2789693
3 D. A. Dombeck, A. N. Khabbaz, F. Collman, T. L. Adelman, and D. W. Tank: Neuron **56** (2007) 43. https://doi.org/10.1016/j.neuron.2007.08.003
4 J. N. D. Kerr and W. Denk: Nat. Rev. Neurosci. **9** (2008) 195. https://doi.org/10.1038/nrn2338
5 K. K. Ghosh, L. D. Burns, E. D. Cocker, A. Nimmerjahn, Y. Ziv, A. El Gamal, and M. J. Schnitzer: Nat. Methods **8** (2011) 871. https://doi.org/10.1038/nmeth.1694
6 D. Aharoni and T. M. Hoogland: Front. Cell. Neurosci. **13** (2019). https://doi.org/10.3389/fncel.2019.00141
7 G. Barbera, B. Liang, L. Zhang, Y. Li, and D. T. Lin: J. Neurosci. Methods **323** (2019) 56. https://doi.org/10.1016/j.jneumeth.2019.05.008
8 I. Ferezou, S. Bolea, and C. C. H. Petersen: Neuron **50** (2006) 617. https://doi.org/10.1016/j.neuron.2006.03.043
9 S. Turtaev, I. T. Leite, T. Altwegg-Boussac, J. M. P. Pakan, N. L. Rochefort, and T. Čižmár: Light Sci. Appl. **7** (2018) 92. https://doi.org/10.1038/s41377-018-0094-x
10 D. C. Ng, T. Tokuda, A. Yamamoto, M. Matsuo, M. Nunoshita, H. Tamura, Y. Ishikawa, S. Shiosaka, and J. Ohta: Sens. Actuators, B **119** (2006) 262. https://doi.org/10.1016/j.snb.2005.12.020
11 J. Ohta, A. Tagawa, H. Minami, T. Noda, K. Sasagawa, T. Tokuda, Y. Hatanaka, Y. Ishikawa, H. Tamura, and S. Shiosaka: Proc. 31st Annu. Int. Conf. IEEE Eng. Med. Biol. Soc. Eng. Futur. Biomed. EMBC 2009 (IEEE, 2009) 5887–5890.
12 J. Ohta, T. Tokuda, K. Sasagawa, and T. Noda: Sensors **9** (2009) 9073. https://doi.org/10.3390/s91109073
13 M. Haruta, C. Kitsumoto, Y. Sunaga, H. Takehara, T. S. Noda, K. Sasagawa, T. Tokuda, and J. Ohta: Jpn. J. Appl. Phys. **53** (2014) 04EL05. https://doi.org/10.7567/JJAP.53.04EL05
14 K. Sasagawa, T. Yamaguchi, M. Haruta, Y. Sunaga, H. Takehara, H. Takehara, T. Noda, T. Tokuda, and J. Ohta: IEEE Trans. Electron Devices **63** (2016) 215. https://doi.org/10.1109/TED.2015.2454435
15 T. Yamaguchi, H. Takehara, Y. Sunaga, M. Haruta, M. Motoyama, Y. Ohta, T. Noda, K. Sasagawa, T. Tokuda, and J. Ohta: Jpn. J. Appl. Phys. **55** (2016) 04EM02. https://doi.org/10.7567/JJAP.55.04EM02
16 Y. Sunaga, H. Yamaura, M. Haruta, T. Yamaguchi, M. Motoyama, Y. Ohta, H. Takehara, T. Noda, K. Sasagawa, T. Tokuda, Y. Yoshimura, and J. Ohta: Jpn. J. Appl. Phys. **55** (2016) 03DF02. https://doi.org/10.7567/JJAP.55.03DF02
17 T. Kobayashi, M. Haruta, K. Sasagawa, M. Matsumata, K. Eizumi, C. Kitsumoto, M. Motoyama, Y. Maezawa, Y. Ohta, T. Noda, T. Tokuda, Y. Ishikawa, and J. Ohta: Sci. Rep. **6** (2016) 21247. https://doi.org/10.1038/srep21247
18 J. Ohta, Y. Ohta, H. Takehara, T. Noda, K. Sasagawa, T. Tokuda, M. Haruta, T. Kobayashi, Y. M. Akay, and M. Akay: Proc. IEEE **105** (2017) 158. https://doi.org/10.1109/JPROC.2016.2585585
19 K. Sugie, K. Sasagawa, M. C. Guinto, M. Haruta, T. Tokuda, and J. Ohta: Electron. Lett. **55** (2019) 729. https://doi.org/10.1049/el.2019.1031
20 M. Haruta, Y. Kurauchi, M. Ohsawa, C. Inami, R. Tanaka, K. Sugie, A. Kimura, Y. Ohta, T. Noda, K. Sasagawa, T. Tokuda, H. Katsuki, and J. Ohta: Biomed. Opt. Express **10** (2019) 1557. https://doi.org/10.1364/BOE.10.001557
21 E. Rustami, K. Sasagawa, K. Sugie, Y. Ohta, M. Haruta, T. Noda, T. Tokuda, and J. Ohta: IEEE Trans. Circuits Syst. I Regul. Pap. **67** (2020) 1082. https://doi.org/10.1109/TCSI.2019.2959592

22 R. Rebusi, J. P. Olorocisimo, J. Briones, Y. Ohta, M. Haruta, H. Takehara, H. Tashiro, K. Sasagawa, and J. Ohta: Front. Neurosci. **15** (2021). https://doi.org/10.3389/fnins.2021.667708
23 T. Pakpuwadon, K. Sasagawa, M. C. Guinto, Y. Ohta, M. Haruta, H. Takehara, H. Tashiro, and J. Ohta: Front. Neurosci. **15** (2021). https://doi.org/10.3389/fnins.2021.667932
24 M. C. Guinto, M. Haruta, Y. Kurauchi, T. Saigo, K. Kurasawa, S. Ryu, Y. Ohta, M. Kawahara, H. Takehara, H. Tashiro, K. Sasagawa, H. Katsuki, and J. Ohta: J. Biomed. Opt. **27** (2022) 26501. https://doi.org/10.1117/1.JBO.27.2.026501
25 K. Naganuma, Y. Ohta, T. E. Murakami, R. Okada, M. C. Guinto, H. Takehara, M. Haruta, H. Tashiro, K. Sasagawa, Y. Sunaga, Y. M. Akay, M. Akay, and J. Ohta: Sens. Mater. **34** (2022) 1561. https://doi.org/10.18494/SAM3710
26 K. Sugie, K. Sasagawa, R. Okada, Y. Ohta, H. Takehara, M. Haruta, H. Tashiro, and J. Ohta: Sens. Mater. (2022) (published online)
27 L. Akbar, V. C. Castillo, J. P. Olorocisimo, Y. Ohta, M. Kawahara, H. Takehara, M. Haruta, H. Tashiro, K. Sasagawa, M. Ohsawa, Y. M. Akay, M. Akay, and J. Ohta: Int. J. Mol. Sci. **24** (2023) 6654. https://doi.org/10.3390/ijms24076654
28 A. J. P. Theuwissen: Solid. State. Electron. **52** (2008) 1401. https://doi.org/10.1016/j.sse.2008.04.012
29 A. Steinzeig, D. Molotkov, and E. Castrén: PLoS One **12** (2017) 1. https://doi.org/10.1371/journal.pone.0181788

About the Authors

Ronnakorn Siwadamrongpong received his B.E. degree in electrical engineering from Chulalongkorn University, Thailand, in 2018 and his M.E. degree from the Nara Institute of Technology (NAIST), Japan. He is currently pursuing his Ph.D. degree at Photonic Device Science Laboratory, NAIST. His research interests include embedded systems, chemical sensors, and implantable devices. (ronnakorn.siwadamrongpong.rh9@ms.naist.jp)

Yoshinori Sunaga received his B.E. degree from Chiba University, Japan, in 2012 and M.E. and Ph.D. degrees from the Graduate School of Materials Science, Nara Institute of Science and Technology (NAIST), Japan, in 2014 and 2017, respectively. In 2017, he joined NAIST as a postdoctoral fellow and began collaborative research between NAIST and the University of Houston. In 2019, he joined the University of Houston as a postdoctoral fellow. In 2022, he joined NAIST as a postdoctoral fellow. He is interested in developing novel devices for observing and assessing brain activity in animals to reveal new brain mechanisms. (sunaga.yoshinori@ms.naist.jp)

Kiyotaka Sasagawa received his B.S. degree from Kyoto University in 1999 and his M.E. and Ph.D. degrees in materials science from NAIST, Japan, in 2001 and 2004, respectively. Subsequently, he became a researcher at the National Institute of Information and Communications Technology in Tokyo, Japan. In 2008, he joined NAIST as an assistant professor and became an associate professor in 2019. His research interests include bioimaging, biosensing, and electromagnetic field imaging. (sasagawa@ms.naist.jp)

Yasumi Ohta received her B.S. degree in physics from Nara Women's University in 1984. She enrolled in the Faculty of Science at Kyoto University in 2004 and switched to a Master's program at the Graduate School of Science, Kyoto University, in 2006. She received her M.S. and Ph.D. degrees in biophysics from Kyoto University, Kyoto, Japan, in 2008 and 2011, respectively. From 1984 to 1986, she worked at Mitsubishi Electric Corp. in Hyogo, Japan. In 2011, she joined the Nara Institute of Science and Technology (NAIST) in Nara, Japan, as a postdoctoral fellow. Her research interests include implantable bioimaging CMOS sensors and neuroscience.
(ohtay@ms.naist.jp)

Hironari Takehara received his ME degree in applied chemistry from Kansai University, Osaka, Japan, in 1986, and his Ph.D. degree in materials science from the Nara Institute of Science and Technology (NAIST), Nara, Japan, in 2015. From 1986 to 2012, he was a semiconductor process engineer at Panasonic Corporation, Kyoto, Japan. In 2015 and 2019, he joined NAIST as a postdoctoral fellow and assistant professor, respectively. His current research interests involve CMOS image sensors and bioimaging.
(t-hironari@ms.naist.jp)

Makito Haruta received his B.E. degree in bioscience and biotechnology from Okayama University, Okayama, Japan, in 2009, and his M.S. degree in biological science and Dr. Eng. degree in material science from Nara Institute of Science and Technology (NAIST), Nara, Japan, in 2011 and 2014, respectively. He was a postdoctoral fellow with NAIST from 2014 to 2016. He joined the Institute for Research Initiatives, NAIST, in 2016, as a project assistant professor. In 2019, he joined the Graduate School of Science and Technology, NAIST, as an assistant professor. In 2023, he became an associate professor at the Faculty of Science and Engineering, Chitose Institute of Science and Technology, and since 2023, he has been a guest associate professor at NAIST. His research interests include CMOS imaging and flexible implantable devices for understanding biological functions.
(m-haruta@photon.chitose.ac.jp)

Hiroyuki Tashiro received his B.E. and M.E. degrees in electrical and electronic engineering from Toyohashi University of Technology (TUT), Aichi, Japan, in 1994 and 1996, respectively. He received his Ph.D. in engineering from Nara Institute of Science and Technology (NAIST), Nara, Japan, in 2017. In 1998, he joined Nidek Co., Ltd., Aichi, Japan, where he worked on the research and development of ophthalmic surgical systems and retinal prostheses. In 2004, he became an assistant professor at the Faculty of Medical Sciences, Kyushu University, Fukuoka, Japan and has been an associate professor at NAIST since 2019. His research interests include artificial vision and neural interfaces.
(tashiro.hiroyuki.289@m.kyushu-u.ac.jp)

Jun Ohta received his B.E., M.E., and Dr. Eng. degrees in applied physics from The University of Tokyo, Japan, in 1981, 1983, and 1992, respectively. In 1983, he joined Mitsubishi Electric Corporation, Hyogo, Japan. From 1992 to 1993, he was a visiting scientist at the Optoelectronics Computing Systems Center at the University of Colorado, Boulder. In 1998, he joined the Graduate School of Materials Science, Nara Institute of Science and Technology (NAIST), Nara, Japan, as an associate professor, and was appointed a professor in 2004. His current research interests include smart CMOS image sensors for biomedical applications and retinal prosthetic devices. He is a Fellow of IEEE, the Japan Society of Applied Physics, and the Institute of Image, Information, and Television Engineers. (ohta@ms.naist.jp)